

MODEL OF A MAGNETIC ACTUATOR AS AN EXTERNAL EXCITATION SOURCE ON ROTATING MACHINERY

Ricardo Ugliara Mendes, rumqld@gmail.com
Kátia Lucchesi Cavalca, katia@fem.unicamp.br
Efrain Araujo Perini, efrainperini@gmail.com
Luiz Otávio Saraiva Ferreira, lotavio@fem.unicamp.br

University of Campinas
Faculty of Mechanical Engineering
Department of Mechanical Design
200, Mendeileiev st., Campinas - São Paulo - 13083-970

Abstract. *Rotating machines have a wide range of application such as airplanes, factories, laboratories and power plants. These applications contain shafts rotating at high speeds that must have high trust levels. Thus the dynamic behavior of these pumps and turbines is desired to design efficient maintenance programs to suddenly avoid manufacturing break-off. Lately, with computers aid designs, shafts finite element models including bearings, discs, seals and couplings have been developed. Through these models the machines behavior can be predicted, allowing optimized design based on the critical speeds calculus and oil instabilities simulations. This information provides the basis for controllers development in order to reduce vibrations during the machines start-up and acceleration or deceleration through the critical speeds, or even to control oil instabilities. In order to keep confidence during operation, the predictive maintenance comes straightforward to the necessity of monitoring these systems, trying to predict future failures. One of the most applied techniques for this purpose is the modal analysis. It consists of applying a perturbation force into the system and then to measure its response. However, there is a difficulty that brings limitations to the excitation of systems with rotating shafts when using impact hammers or shakers, once due to friction, undesired tangential forces and noise can be acting on the system. Therefore, the study of a non-contact technique of external excitation becomes of high interest. In this sense, the present work deals with the study and development of a finite element model for rotating machines using a magnetic actuator as source of external excitation, focusing on the model response and its interaction with the actuator. It is also presented a comparison between numerical simulations and practical tests obtained from a rotor test rig.*

Keywords: *magnetic actuator; rotating machinery; excitation without contact.*

1. INTRODUCTION

Lately, with computers aid design, a new technic, called finite element model (FEM), was introduced to rotating machinery modeling. In this technic, the continuous shaft is divided into finite elements. The first models used the Euler-Bernoulli beam, whose equations are obtained from the application of the Lagrange equation in a simple beam. Then, the model was expanded to two directions, considering only the shaft translational inertia and its stiffness. A breakthrough in the modeling of rotating machines is shown in Nelson and McVaugh (1976) that studied a model called the Rayleigh beam, which takes into account the rotational inertia of the shaft and the gyroscopic effect, dependent on the shaft rotational speed.

Once obtained a representative model of the shaft, models of the other elements of rotating machines (such bearings, seals, foundations, rotors) should be incorporated in order to study the phenomena inherent to these systems. Nelson (2007) reviewed these phenomena in an informatively way, that is, not going into the equations. Authors considered reference in this area, Vance (1988), Kramer (1993) and Childs (1993), modeled many of the components mentioned above and analyzed their influence on rotor dynamics.

The analysis and comparison between various methods for calculating coefficients of journal bearings was carried out by Silva (2004). Machado and Calvalca (2009) used a finite-difference method to solve the Reynolds equation for multi-lobular bearings, and calculated linear coefficients from the pressure distribution. Castro (2007) studied a non-linear model and calculated non-linear coefficients, also making a calibration of the models using a meta-heuristic adjustment method based on a genetic algorithm.

Non-symmetric rotors or with anisotropy have precession modes which can be forward or backward and, in this sense, Kessler (1999) studied complex modal analysis in order to distinguish these to two modes.

Magnetic actuators are mainly composed of solenoids, coils wound on a core of ferromagnetic material. When a current is applied to the coils, a magnetic field is induced in its ferromagnetic core, generating the magnetic force. The bases of active magnetic bearing (AMB) are magnetic actuators. The main advantages of this bearing on other types of bearings are low maintenance, no lubrication, and thus, the absence of seals and contamination, and the ability to operate in extreme conditions such as very low or high temperatures and vacuum. The AMB has been used in many types of rotating machines, from turbo molecular pumps to steam turbines, due to its wide field of application, both in terms of size and workload. The non-contact between the bearings and the shaft causes the speed of these devices to be

limited only by the fracture properties of the rotor, and not by the bearings, as observed with hydrodynamic and roller bearings (Knospe, 2005).

The works of Chiba et al. (2005) and Malsen (2000) are important references in this area. They deal with the development of magnetic actuators including the differential linearization, where two actuators are placed radially opposed. Once magnetic actuators can generate only attractive forces, this positioning allows applying forces in both ways of the actuator direction and also linearizes the magnetic force.

2. MECHANICAL SYSTEM

The model of the mechanical system, shown in Fig. (1a), consists in the finite element model (Fig. (1b)) of the steel SAE 1030 shaft of 12 mm diameter and 800 mm length, which is split into 21 elements (represented by the red dots). There is also a 94.82 mm diameter and 47.5 mm width disc (represented in red color in Fig. (1b)), which is placed in the center of the shaft. The model also considers the actuator journal placed at 62 mm of the first bearing, of 80 mm length and 40 mm diameter, both made of steel SAE 1020. The system is supported by two hydrodynamic bearings (green triangles in Fig. (1b)) placed 600 mm symmetrically from each other regarding to the middle of the shaft, both with 90 μm clearance, 20 mm width and 30 mm inner diameter. The lubricant used in this mechanical system is the oil AWS 32 from Castrol (ISO VG 32).

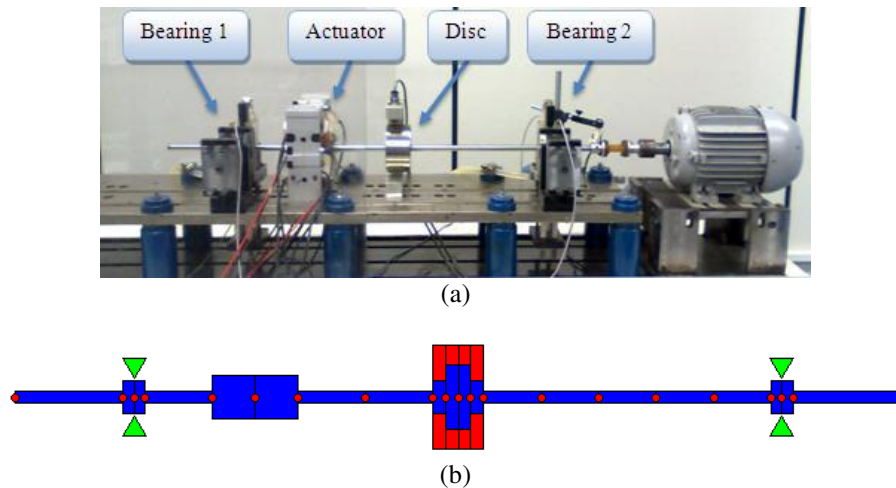


Figure 1. (a) Test Rig; (b) Finite element model of the mechanical system.

The equation of the finite element model can be seen in Eq. (1), where Ω is the rotational speed, M is the mass matrix, G the gyroscopic effect matrix, K the stiffness matrix and C is the structural damping matrix proportional to K by a factor of 2×10^{-4} (estimated value for steel shafts - Weiming and Novak, 1996). Also from Eq. (2), the matrix M is obtained from the sum of other two matrices: the rotatory mass matrix M_R and the translational mass matrix M_T . All the matrices mentioned above were obtained from the work of Nelson and McVaugh (1976). F is the external forces, as the unbalance, from an unbalanced mass and the actuator force; q is the generalized coordinate vector, with two translations and two rotations for each node.

$$[M]\{\ddot{q}(t)\} + ([C] + \Omega[G])\{\dot{q}(t)\} + [K]\{q(t)\} = [F(t)] \quad (1)$$

$$[M] = [M_T] + [M_R] \quad (2)$$

The journal bearings are modeled by equivalent coefficients of damping and stiffness (Fig. (2)) that are added in the corresponding system matrix. The coefficients are evaluated from the pressure distribution, which is obtained by Reynolds equation solution (Eq. (3))

$$\frac{\partial}{\partial y} \left(h^3 \frac{\partial p}{\partial y} \right) + \frac{\partial}{\partial x} \left(h^3 \frac{\partial p}{\partial x} \right) = 6\mu\Omega \frac{\partial h}{\partial y} + 12\mu \frac{\partial h}{\partial t} \quad (3)$$

where x is axial coordinate, y and z are the transversal coordinates, μ is the viscosity of the fluid, h is the fluid film thickness, p pressure and t is the time; and the finite-difference method is used. The coefficients are evaluated from Machado and Cavalca (2009), and their behavior regarding to the rotational speed are shown in Figs. (3) and (4).

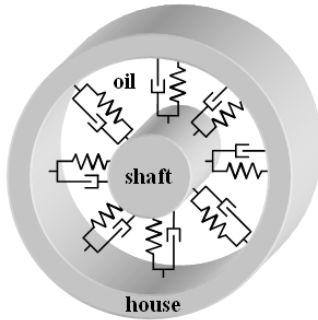


Figure 2. Model of the journal bearing.

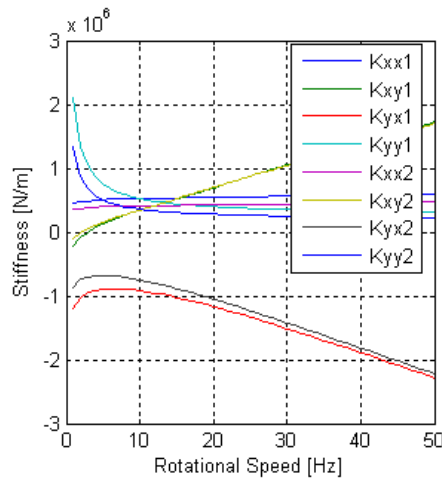


Figure 3. Stiffness coefficients.

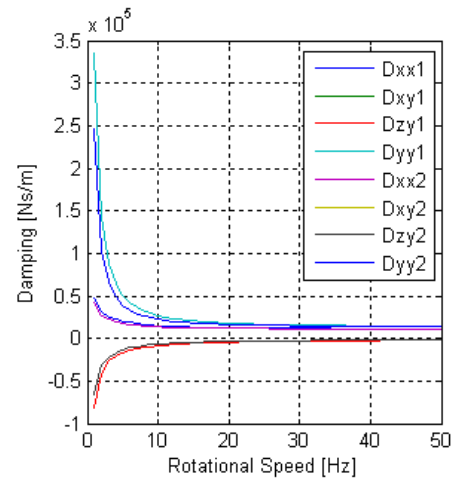


Figure 4. Damping coefficients.

3. MAGNETIC ACTUATOR

The force obtained by a magnetic actuator (Eq. (4)) is proportional to the area of the actuator pole (A) and the magnetic flux density (B), which is given by Eq. (5) (Chiba et al., 2005) and it is proportional to the number of turns in the coils (N), the current (i), the length of the air gap (l_g) and the magnetic permeability of the air (μ_g). Thus, according to Furtado (2008), the control of the actuator force can be made through the magnetic field control as shown in Fig. (5), where B_{ref} is the magnetic field correspondent to the reference force which is compared to the magnetic field measurement made by the hall sensor. This comparison is the proportional controller input. The output voltage of the controller is transformed into the correspondent current by the PWM amplifier, and sent to the coils of the actuator, generating the magnetic force F_m .

$$F_m = -\frac{B^2 \cdot A}{\mu_g} \quad (4)$$

$$B = \frac{\mu_g \cdot N \cdot i}{2 \cdot l_g} \quad (5)$$

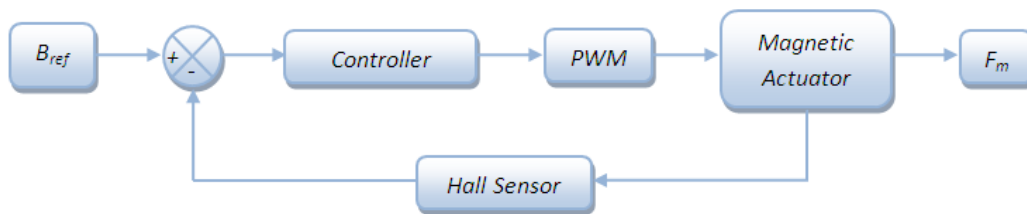


Figure 5. Magnetic system diagram.

3.1. Finite Element Model

A finite element model for the actuator magnetic field was created using the commercial software Ansys®. With this model, it was possible to study design characteristics of the actuator, such as the coils distribution in the actuator core, the magnetic field behavior and the resultant force obtained for different pole geometries. The magnetic force (F_m) acting in a component is calculated integrating the Maxwell Stress Tensor (MST) on its surface as in Eqs. (6) and (7); where s is the surface area of the element, n_i is the component of unit normal in i -direction and T is the magnetic tensor.

$$\{F_m\} = \frac{1}{\mu_g} \int_s \begin{bmatrix} T_{11} & T_{12} & T_{13} \\ T_{21} & T_{22} & T_{23} \\ T_{31} & T_{32} & T_{33} \end{bmatrix} \begin{Bmatrix} n_1 \\ n_2 \\ n_3 \end{Bmatrix} ds \quad (6)$$

$$\begin{cases} T_{ii} = B_i^2 - \frac{1}{2}|B|^2 \\ T_{ij} = B_i B_j \end{cases} \quad (7)$$

3.2. Coils Distribution in the Actuator Core

Although Eq. (5) presents the influence of the number of coils (N) and the current (i) in the evaluation of the magnetic flux density (B), it does not provide any information about the coils distribution in the actuator core. This distribution does not affect the evaluation of the magnetic force using Eq. (4), but, when using a finite element model (FEM), a significant influence can be seen.

Figure (6) shows the magnetic flux density obtained with the actuator containing one coil with 830 turns, located in the core right arm, subjected to a current of 3A. Figure (7) shows the same coil divided in two, one in each arm of the core, connected in series. For this simulation it was used an air-gap of 2.5 mm and the area of the pole equal to 500 mm². Either the actuator pole and the journal were simulated as plane surfaces.

In Fig. (6) is possible to notice that the magnetic flux density was stronger in the region near the coil. As the magnetic force is proportional to the magnetic flux density, an unbalance occurs, generating a more intense force in one of the poles. In Fig. (7) there is a symmetry in the force due to the symmetry in the magnetic flux density distribution. Thus, in the case of Fig. (7), the magnetic force occurs to be uniform in both poles, minimizing momentum effects in the center of the actuator, as concluded in the studies of Castro et al. (2007).

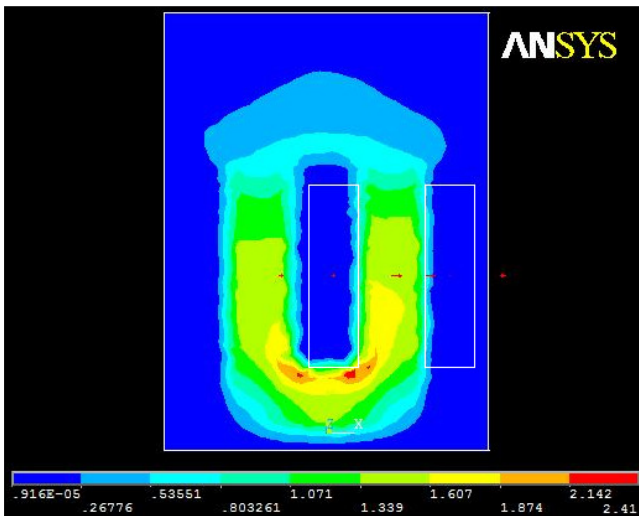


Figure 6. Magnetic Flux Density – one coil at the right arm of the core.

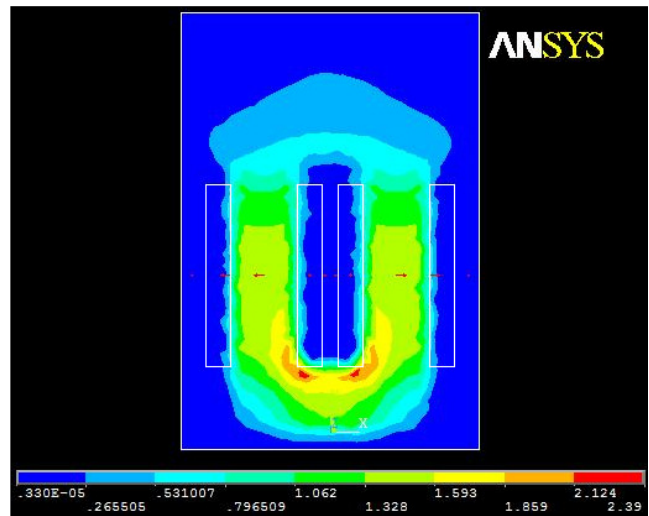


Figure 7. Magnetic Flux Density – one coil at each arm of the core.

3.3. Influence of the Pole Geometry

One of the approaches used to evaluate the magnetic force, using Eq. (4), is considering a constant air-gap and an uniform distribution of the magnetic flux density in the actuator pole. However, it can be shown in the FEM simulation that this is not the real behavior of the magnetic field and, specially in the cases where the air-gap is not constant in the whole extension of the pole, the usage of the Eq. (4) may be compromised.

In this sense, three finite element models with different geometries were created to verify the influence of the surfaces (from the pole and the journal of the actuator) in the calculus of the magnetic force, either using the Maxwell Stress Tensor and the Eq. (4).

The three geometries are presented in Fig. (8): (S1) – plain journal and plain pole, (S2) - circular journal and plain pole and (S3) – circular journal and circular pole. In either cases S1 and S3 the air-gap was kept constant and equal to 2.5 mm. The journal diameter is 40 mm. In the case S2, the thinner region of the air-gap has 2.5 mm.

The evaluated forces for the three geometries using MST are in Tab. (1), as well as the calculation with Eq. (4).

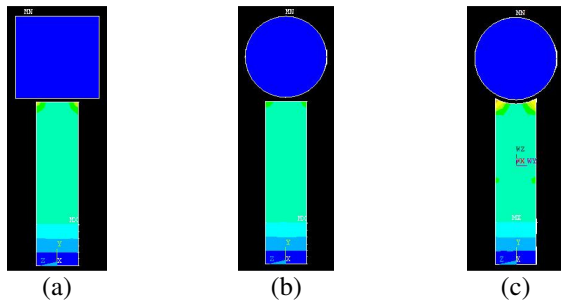


Figure 8. Different geometries studied: (a) plain-plain, (b) plain-circular, (c) circular-circular

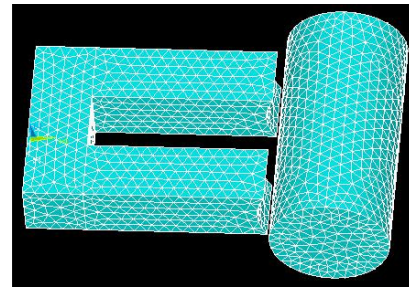


Figure 9. FEM of the geometry S3.

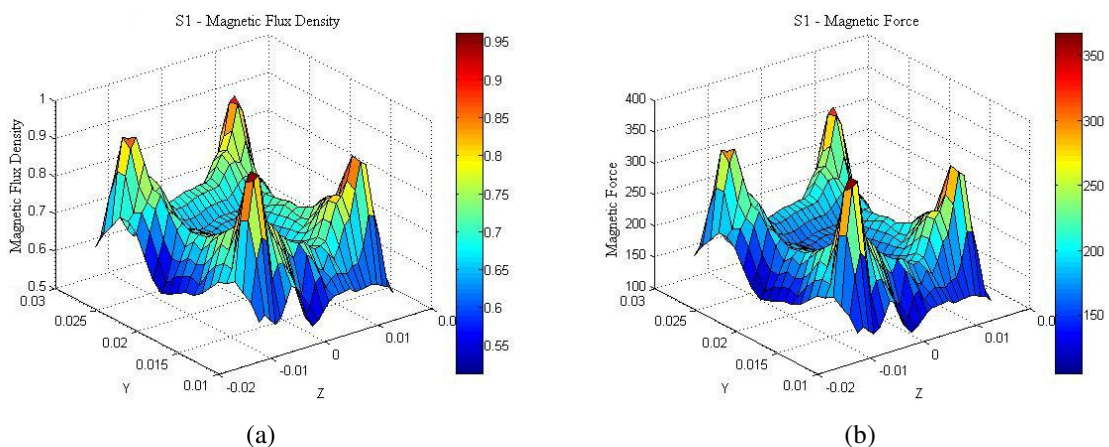
Table 1. Forces obtained by varying the geometry of the actuator FEM.

Geometry	(a) – S1	(b) – S2	(c) – S3
Force (N) - M.S.T.	219,21	94,33	178,99
Force (N) - Eq. (4)	160,97	143,16	181,23

In order to calculate the forces with Eq. (4), the magnetic density flux in the center of the air-gap was used for the three geometries. It can be noticed that the force obtained in the case S2 (plain-circular) was the smallest, because the area of the air-gap with 2.5 mm was reduced, causing higher losses in the rest of the air-gap. The force estimated through Eq. (4) were greater than those calculated by the MST, in this case, because the equation did not consider the geometry and the magnetic field was stronger in the region where the air-gap was smaller, the pole center, as seen in the mapping in Fig. (10c).

In the cases S1 (plain-plain) and S3 (circular-circular), the forces risen, because, as the air-gap was constant, there were fewer losses of the magnetic field. The case S1 presented the biggest magnitudes of forces due to the proximity of the whole area of the journal with the actuator pole, thus the field leakage, that occur as a border effect, found the journal easier than in the case S3. However, the value of the magnetic field in the actuator pole was bigger for the case S3, where a more uniform distribution was found in the pole surface then in the case S1, Figs. (10e) and (10a). This fact explains why the force obtained using Eq. (4) was bigger in the case S3 than in S1. Therefore, the case S3 presented the best estimation of the magnetic force, using Eq. (4), when compared to the value obtained through the numerical simulation.

As the actuator is intended to be used as a source of external excitation in rotating systems, and as the shaft is circular, the case S3 was adopted as the standard, being used in experimental setup and also for a more refined mapping of the magnetic flux density near the actuator pole. Figure (9) shows the FEM used for analysis of the magnetic actuator with the circular-circular geometry.



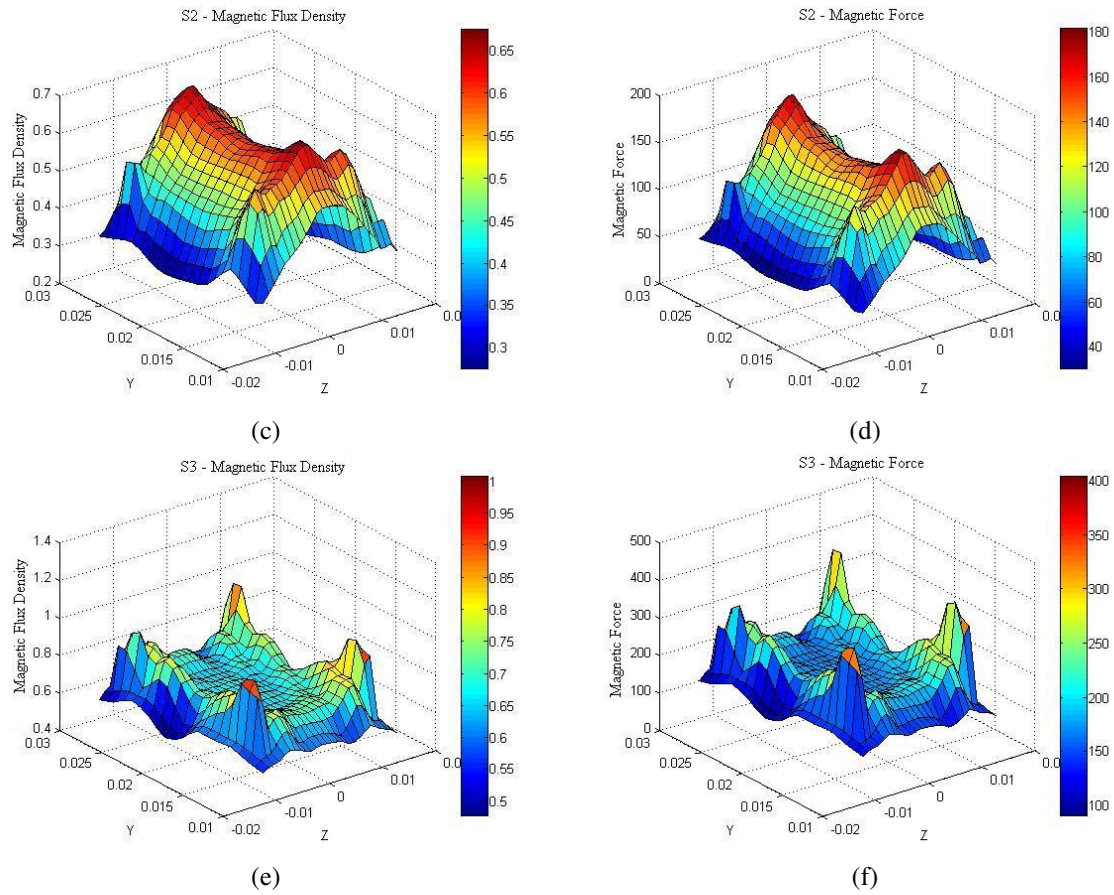


Figure 10. Magnetic flux density (MFD) and magnetic force maps for the three evaluated geometries: a) plain-plain MFD, b) plain-plain magnetic force, c) plain-circular MFD, d) plain-circular magnetic force, e) circular-circular MFD, f) circular-circular magnetic force.

3.4. Influence of the Hall Sensor Positioning

In order to estimate the experimental value of the magnetic force the Eq (4) was used. In this equation, the force is proportional to the magnetic flux density and, as this relation is of quadratic order, any variation has significant influence on the calculations.

To obtain the magnetic flux density hall sensors were used and, as these sensors have a sensitive 0.04 mm^2 area, its positioning may affect the calculation of the force if the field is not constant within the air-gap. In this sense, the magnetic field and the magnetic force were mapped in the air-gap region. Figures (10a), (10c) and (10e) show the magnetic flux density in the air-gap region, next to the core, for each of the cases (S1, S2 and S3). While Figs. (10b), (10d) and (10f) show the magnetic force calculated taking as basis the magnetic field distribution for each case. A 1 mm resolution grid was employed in all cases.

At the geometries S1 and S3, there was the influence of a border effect, where the magnetic flux density was higher. Particularly in geometry S2, this effect was masked because, as the air-gap was smaller in the center of the pole, the concentration of the magnetic field in this area was greater. As the objective of the mapping was the study of the hall sensor positioning influence, and not the study of the border effect, it was taken into account only the pole central region (9 mm x 9 mm), where the magnetic field had a more homogenous distribution (Fig. (11)). It was used geometry S3, as explained before.

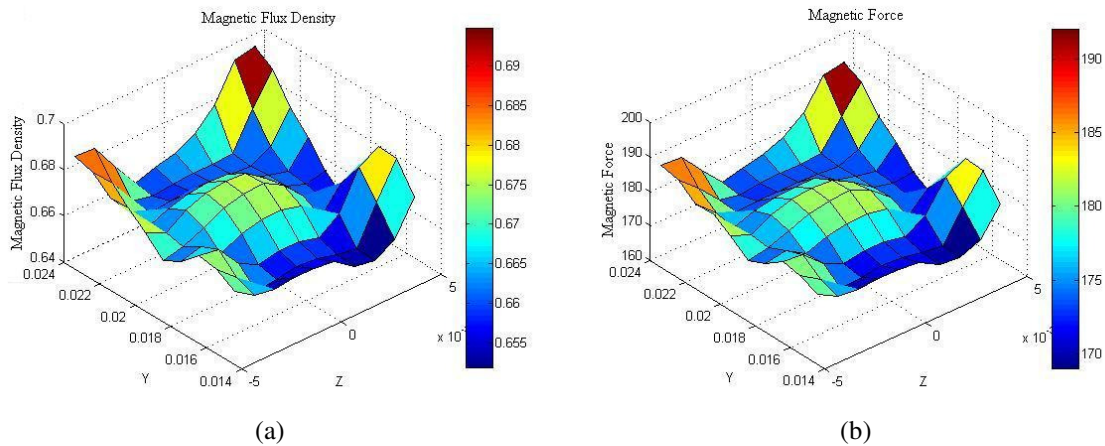


Figure 11. Magnetic field and magnetic force maps in the actuator pole center (circular-circular pole).

It can be noticed that, in the central region, there were smaller variations in the magnetic flux density than occurs when it is analyzed towards the edges. One explanation for this fact is that, in the central region, the field lines tend to have a more homogeneous behavior. Therefore, for this case, the variation of the force, using the maximum and minimum values, was approximately 12%. This variation suggests positioning the sensor in the central region of the actuator pole, which gave a very effective estimative, as seen in Tab. (1). Also comparing the results of the force calculated with MST and Eq. (4), for the geometry S3 in Tab. (1), the error was only 1.25%, which is in agreement with Aenis et al. (2002), which concluded that using a hall sensor in the center of the actuator pole can reduce the force measurement error to 2%, and, if using one hall sensor in each pole of the actuator, it can be reduced to only 1%.

4. EXPERIMENTAL SETUP

The experimental setup is presented in Fig. (12). The mass displacements measurement were taken by two proximity sensors from “CE - Turck”, and the journal bearings displacements, by four proximity sensors from “Bently Nevada”. The six sensors were used with their respective signal conditioners and all of their signals pass through two filters before been acquired: a DC offset filter and an anti-aliasing filter. The interface between the computer and the system is made by a general purpose control card AT-MIO-16-E2 from “National Instruments”.

The test rig also has a triphasic motor and a frequency inverter CFW-08, both from “WEG”, and the communication with the PC is made through a serial communication module XC8, also from “WEG”.

In order to amplify the signal from the controllers, a PWM amplifier 4-Q-DC-Servoamplifier from “MAXON” was used. The amplifier works in the current control mode, converting the input voltage in the desired current, because, as Eq. (5) shows, the magnetic field is not proportional to the voltage, but to the current. Its calibration curve was measured and it is presented in Fig. (13).

In ferromagnetic materials, the magnetic dipoles are aligned through the application of an external magnetic field. This alignment depends on the applied external magnetic field and the type of ferromagnetic material. The applied external field influences the magnetic dipoles that were randomly distributed, aligning them. Thus, the resultant magnetic field, due to the applied external magnetic field and the dipoles alignment, becomes larger than the applied external field, resulting on the amplification of its magnitude.

The external magnetic field is increased as higher is the resultant magnetic field, until the total orientation of the dipoles of the ferromagnetic material. Beyond this point, an increase of the external magnetic field does not produce a substantial increase in the resultant field, once that only the portion related to the external field increases. When this behavior is observed, it is said that the ferromagnetic material has reached its magnetic saturation.

Therefore, knowing the behavior of the ferromagnetic material, it is important to know until which value the increasing of the current in the coils provides a substantial increase at the magnetic field. The curve that shows this behavior is called hysteresis curve. The hysteresis curve was obtained experimentally for 3 values of air-gaps (2, 2.5 and 4.5 mm) as shown in Fig. (14). In the case of 2 mm air-gap, the beginning of the saturation can be observed, for 2.5 mm, there is only a tendency to the saturation, and for 4.5 mm, the tendency to the saturation can no longer be observed in the analyzed interval. This occurs because the air has an extremely low magnetic permeability, thus, with a larger air-gap, there are higher losses of magnetic field, which decreases the magnetic field in the magnetic circuit.

A CAD model of the actuator structure was made with the commercial software Pro-Engineer (Fig. (15a)) in order to determine its natural frequencies. The first two natural modes are presented in Figs. (15b) and (15c), and correspond to the frequencies of 576 Hz and 774 Hz. Thus, these frequencies are beyond the operational range, which is up to 60 Hz.

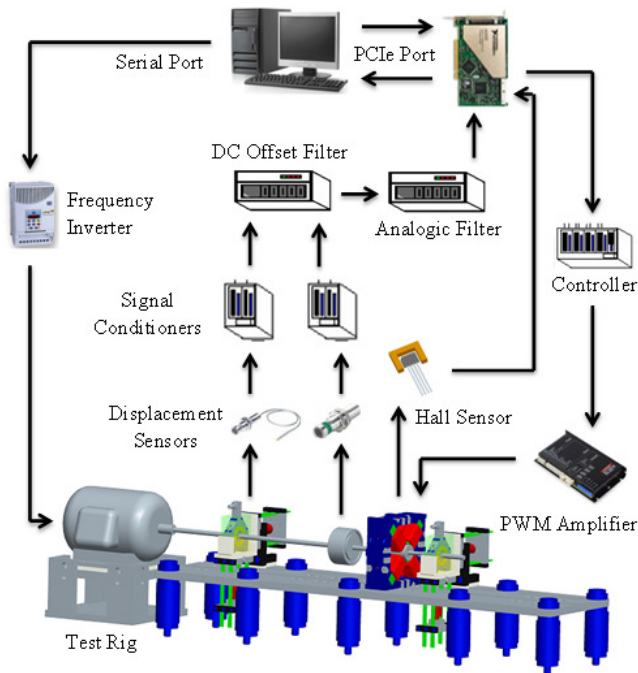


Figure 12. Experimental Setup.

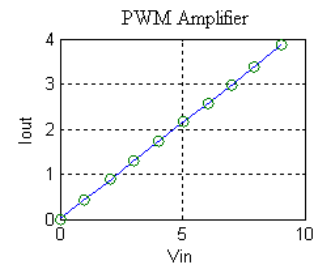


Figure 13. Amplifier calibration curve.

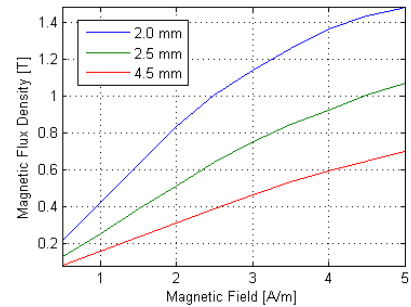


Figure 14. Hysteresis Curve.

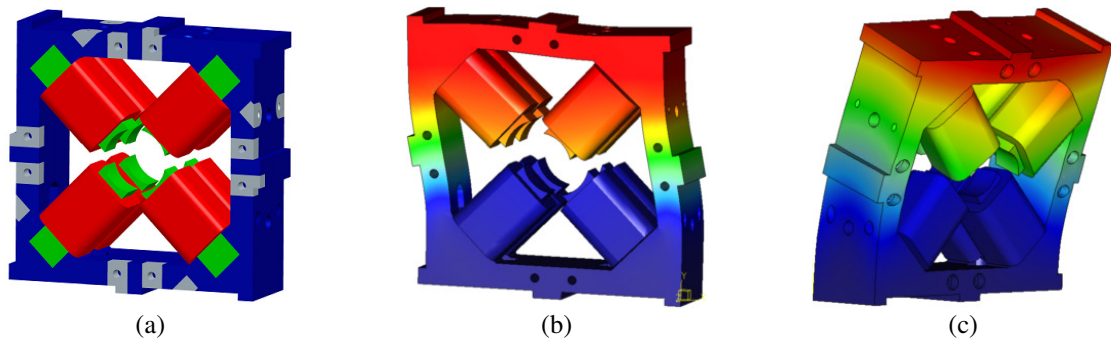


Figure 15. (a) actuator CAD model; (b) first natural mode at 576 Hz; (c) second natural mode at 774 Hz.

5. SIMULATED AND EXPERIMENTAL RESULTS

In rotor dynamics, the precession movements (also called whirl), which causes the orbits, can be forward, if they occur in the same direction of the rotor spin, or backward, if in the opposite direction. In order to separate these two movements in the spectrum, the concept of the Fourier transform of real signals can be expanded for complex signals, using the complex exponential, as presented in the work of Goldman and Muszynska (1999). Thus, the positive part of the spectrum presents the forward precession and, the negative part, the backward precession. The direction of the peak with higher amplitude determines if the motion is predominantly forward or backward.

To validate the model, the frequency spectrum of the disc displacement from the numerical simulation and the practical test were compared. The comparison was accomplished for two different rotational speeds (30 and 35 Hz) and three excitation frequencies of the magnetic actuator (20, 25 and 30 Hz). In all cases it was used a sinusoidal force of 10 N in one of the actuator directions, and the actuator air-gap was 1.7 mm. The red lines (Fig. (16)) refer to the experimental results and the blue lines, to the simulated results.

Peaks due to the unbalance appear in all the cases, always in the positive frequencies of the rotational speed, because the unbalance is a synchronous force. The small peaks at the same frequencies, but in the negative parts of the spectrums, occur because of the anisotropy of the system (Kramer, 1993); in this case, due to the hydrodynamic bearings. The damped peaks around 23 Hz in both sides of the spectrum, where also occur phase shifts, represent the first critical speed of the system, the forward and the backward components.

In the cases of Figs. (16a) and (16b), the excitation peaks at the frequency of 20 Hz were highest in the positive part of the spectrum, thus the displacements were predominantly forward. When the excitation frequency was 25 Hz (Figs.

(16c) and (16d)), the peaks were highest in the negative part of the spectrum, featuring predominantly backward displacements.

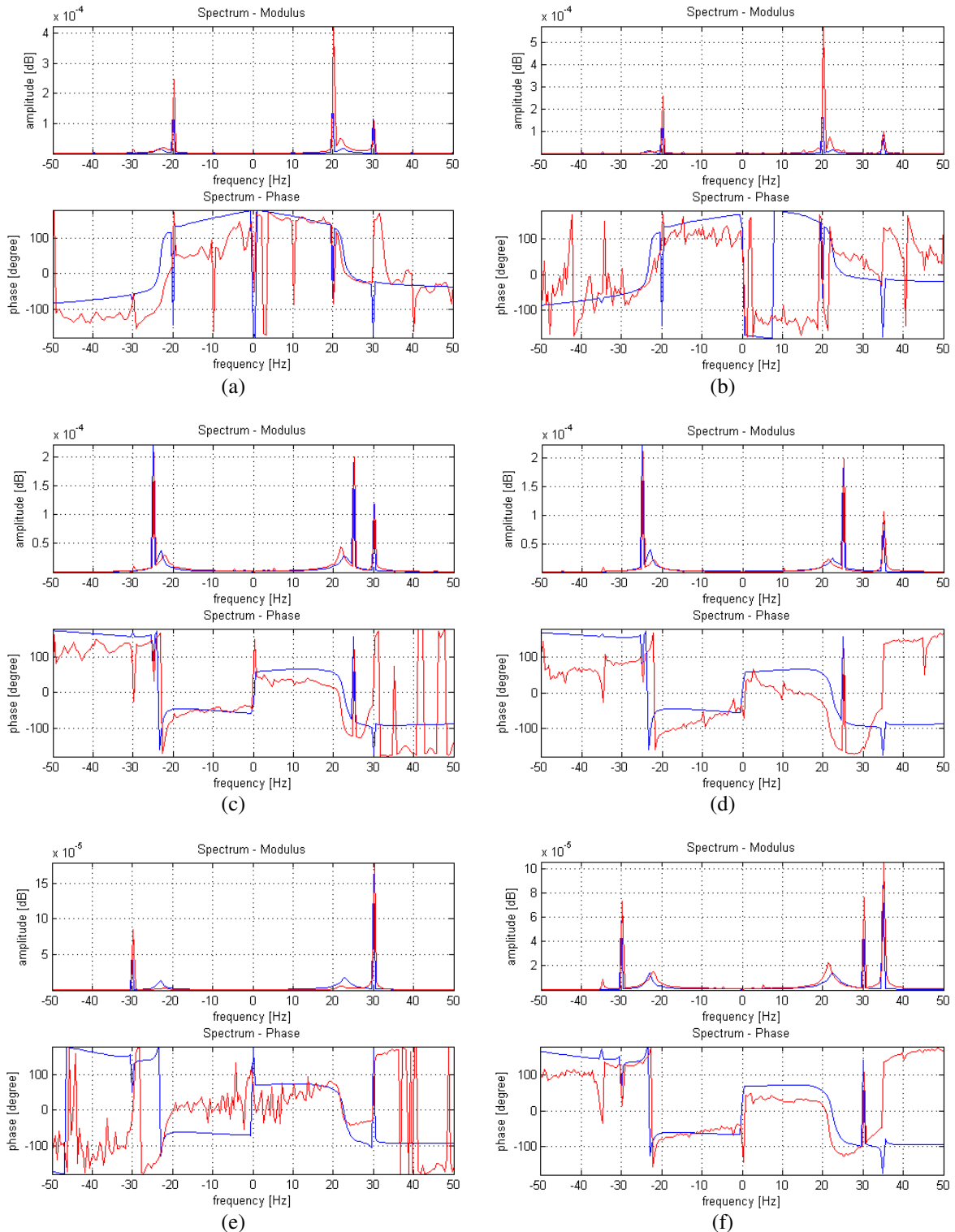


Figure 16. Comparison between numerical simulations (blue) and practical tests obtained from the test rig (red): (a) rotation 30 Hz, excitation 20 Hz; (b) rotation 35 Hz, excitation 20 Hz; (c) rotation 30 Hz, excitation 25 Hz; (d) rotation 35 Hz, excitation 25 Hz; (e) rotation 30 Hz, excitation 30 Hz; (f) rotation 35 Hz, excitation 30 Hz.

This fact occurs because, even though the critical velocities are very close to each other, they do not overlap due to the anisotropy of the system. Thus, the smaller critical velocity, related to the forward precession, is closer to excitation of 20 Hz, and the critical velocity related to the backward precession is closer to the excitation frequency of 25 Hz.

Finally, when the excitation frequency was 30 Hz, Figs. (16e) and (16f), i.e. more distant from both critical velocities, the peaks become dominant at the rotation speed, therefore, the unbalance prevails, and the forward precession predominates over the backward one.

6. CONCLUSIONS

The FEM simulations of the magnetic actuator provided important information to its design, not taken into account by the analytical models, such as the coils turns distribution and the geometry of the actuator poles. These simulations also showed that the use of hall sensors is very effective to estimate the magnetic force.

It is a common sense that there is a difficulty in obtaining models that accurately represent real systems, this fact comes from the lack of parameters inherent in the system, approximations and simplifications of the analytical models, making necessary the use of model adjustment technics. However, the study of such technics is an extensive field of research, which is not the focus of the present work. Thus, the comparison between the experimental and simulated results showed the program satisfactorily represents the system, especially considering that no adjustment methods were used. These results also showed that the magnetic actuator can be used as an external excitation source in modal analysis or vibration control at the critical velocities of the shaft or at the oil- instability, once it is capable to apply the desired force at the desired frequency, exciting either forward or backward whirling frequencies.

7. ACKNOWLEDGEMENTS

The authors would like to thank Fapesp, CAPES and CNPq for the financial support to this research.

8. REFERENCES

- Aenis, M., Knopf, E. and Nordmann, R., 2002, "Active Magnetic Bearings for the Identification and Fault Diagnosis in Turbomachinery", *Mechatronics*, v.12, p.1011-1021.
- Castro, H.F., 2007, "Análise de Mancais Hidrodinâmicos em Rotores sob Instabilidade Fluido-Induzida", 176p., Dissertation (Ph.D.) – Faculty of Mechanical Engineering – University of Campinas, Campinas – SP, Brazil.
- Castro, H.F., Furtado, R.M., Cavalca, K.L., Pederiva, R., Butzek, N. and Nordmann, R., 2007, "Experimental Performance Evaluation of Magnetic Actuator used in Rotating Machinery Analysis", *Journal of the Brazilian Society of Mechanical Science & Engineering*, v.29, n.1/93, January-March.
- Chiba, A., Fukao, T., Ishicawa, O., Oshima, M., Takemoto, M. and Dorrell, D.G., 2005, "Magnetic Bearings and Bearingless Drives", Ed. Newnes. 381p.
- Childs, D., 1993, "Turbomachinery Rotordynamics: Phenomena, Modeling, and Analysis", Wiley-Interscience, 496p.
- Furtado, R.M., 2008, "Desenvolvimento de um Atuador Magnético para Excitação sem Contato de Sistemas Rotativos", 113p., Dissertation (Ph.D.) – Faculty of Mechanical Engineering – University of Campinas, Campinas – SP, Brazil.
- Goldman, P. and Muszynska, A., 1999, "Application of Full Spectrum to Rotating Machinery Diagnostics", *Orbit*, First Quarter, p.17-21.
- Kessler, C. L., 1999, "Complex Modal Analysis of Rotating Machinery", 106p, Dissertation (Ph.D.) - University of Cincinnati, Cincinnati – OH, United States.
- Knospe, C.R., 2005, "Active Magnetic Bearings for Machining Applications", *Control Engineering Practice*, v.15, p.307-313.
- Kramer, E., 1993, "Dynamics of Rotors and Foundations", New York: Springer-Verlag, Berlin Heidelberg, 383p.
- Machado, T.H. and Cavalca, K.L., 2009, "Evaluation of Dynamic Coefficients of Fluid Journal Bearings with Different Geometries", *Proceedings of 20th Brazilian Congress of Mechanical Engineering - COBEM*, November 15-20, Gramado – SP, Brazil.
- Maslen, E., 2000, "Magnetic Bearings". University of Virginia, 233p.
- Nelson, F.D., 2007, "Rotor Dynamics Without Equations", *International Journal of COMADEM*, v.10, n.3, p.2-10.
- Nelson, H.D. and McVaugh, J.M., 1976, "The Dynamics of Rotor-Bearing Systems Using Finite Elements", *Journal of Engineering for Industry*, p.593-600.
- Silva, E.L., 2004, "Dinâmica de Rotore: Modelo Matemático de Mancais Hidrodinâmicos", 110p. Dissertation (M.Sc.) - Federal University of Paraná, Curitiba-PR, Brazil.
- Vance, J.M., 1988, "Rotordynamics of Turbomachinery", Wiley-Interscience, 400p.
- Weiming, L. and Novak, M., 1996, "Dynamic behaviour of turbine-generator-foundation systems", *Earthquake Engineering and Structural Dynamics*, v.24, n.3, p.339-360.

9. RESPONSIBILITY NOTICE

The authors are the only responsible for the printed material included in this paper.